fluids

MDPI

Article

A Validation of the Junction Riemann Problem in Networks of Channels Under Transitory Flow Conditions

Juan Mairal *, Javier Murillo and Pilar Garcia-Navarro

Institute of Engineering Research of Aragon (I3A), University of Zaragoza, C. de Mariano Esquillor Gomez, 50018 Zaragoza, Spain; Javier.Murillo@unizar.es (J.M.); pigar@unizar.es (P.G.-N.)
* Correspondence: mairal@unizar.es

Abstract: Transitory states and supercritical regimes in channel junctions have been challenging to model using 1D models, and it has been common to resort to 2D models to locally solve networks of channels. In this paper, we present a methodology based on the Junction Riemann Problem that manages to include supercritical solutions by making use of suitable limiting coefficients. The method is compared against a pure 2D model in a series of test cases with challenging geometries that include transitory flow conditions. The results show that the method hereby presented is robust across all regimes and is able to capture the main features of wave propagation along a network of channels.

Keywords: shallow water; junction; network; transitory; supercritical; Riemann problem

1. Introduction

The flow of water in channels has often been modeled using one-dimensional (1D) formulations, where only one spatial coordinate is deemed important. Water channels [1,2], gas pipes [3–5], and blood vessels [6–10] are a few examples where these models have been successfully applied. The usefulness of this type of approximation lies in the reduction in the complexity of the models and methods and, more importantly, in the number of computational cells. Thus, 1D models are an excellent choice when the domain of interest is mostly laid in one direction, as the loss of information caused by dimension reduction is compensated by the enormous increase in efficiency, which in turn allows for faster simulations, higher resolutions, or larger domains [11]. Thus, robust methods to solve wave dynamics and propagation in networks are necessary to include other relevant phenomena, such as pollutant or solute transport [12].

The subject of study in this paper are networks of open channels, where free-surface flow is modeled by the shallow water equations, with a source term to account for changes in bed level, channel width, and friction. While there are many well-established methods, this system of hyperbolic partial differential equations models flow in the channels themselves, and their coupling at the junctions requires special consideration. Traditionally, in the 1D approximation, basic conditions including the equality of water levels have been used [13]. More complicated models have been devised based on momentum loss and recirculation due to the geometry of the junction [14,15].

In other cases, junctions are included as elements of higher dimension (2D) [1,16], but this approach results in a loss of efficiency and is mainly proposed to overcome the shortcoming of pure 1D coupling. Indeed, the conditions used up to this point are typically limited to the subcritical regime and even to relatively slow flows (Fr < 0.35) [17]. Some strategies have been devised to solve junction problems in the supercritical regime, but only for some specific geometries and a general formulation was missing [18–20].

Academic Editors: Kamil Urbanowicz and Juha Videman

Received: 16 January 2025
Revised: 11 February 2025
Accepted: 18 February 2025
Published: 20 February 2025

Citation: Mairal, J.; Murillo, J.; Garcia-Navarro, P. A Validation of the Junction Riemann Problem in Networks of Channels Under Transitory Flow Conditions. *Fluids* **2025**, *10*, 53. https://doi.org/10.3390/fluids10030053

Particularly, reference [1] argued in favor of local 2D elements to represents junctions in 1D networks, showing that a 1D method based on Sherwin's method for blood vessels [21] could not produce accurate results, and would not run altogether in supercritical conditions. In this paper, we showcase a methodology also first used to solve blood vessels [9,10] that is able to solve the junction problem in the supercritical regime.

The proposed strategy in this paper makes use of the Junction Riemann Problem [22,23], a generalization of the Riemann problem to a junction of channels, each initially in a uniform state. The Riemann problem is a well-known [24] initial value problem (IVP) in the theory of hyperbolic systems of PDEs that is the foundation of popular methods [25] to solve them. While these methods often make use of approximate solutions, the coupling of the terminal cells of the channel seeks an exact solution, whose existence has been proven for some configurations [23,26] in the subcritical regime.

The method presented here is coupled to an energy-balanced finite volume (FV) scheme of first-order accuracy that makes use of the Augmented Riemann method to solve for the inter-cell fluxes [27]. It is worth noting that, since solving the Junction Riemann Problem yields the exact solution at the edge of the terminal cell, it can be used in combination with other schemes, even of higher order. The properties of these types of methods are explained in detail in [28], including the complete derivation of an approximate Riemann solver for general hyperbolic systems of equations with non-conservative terms and its application to the shallow water equations in both 1D and 2D.

This paper does not delve into the mathematical theory of the problem, but rather shows its practical application, including supercritical flow conditions. A more detailed explanation is presented in [29], where the different possible combinations of flow regimes and flow orientations are analyzed following the groundwork laid out in [9] for blood vessels. The novelty of this paper is the validation against reference solutions produced in 2D domains through a well-established numerical method [30] that is currently used in practical cases [31]. The emphasis in the test cases is put on the transitory flow conditions by looking at how shock waves propagate through junctions. Thus, we are interested in the accuracy of the method in capturing the long-term behavior of the flow in the network, and not in the details at the junction. It is clear that a 1D method will never be able to capture the complex flow patterns that arise in 2D domains, but it is expected that the method is able to reproduce the main features of the flow to the accuracy of the numerical method.

This paper is organized as follows: The mathematical models and their main equations are given in the next section, followed by a description of the numerical methods used to solved them. Both the 1D model of interest and the 2D model used to validate it are presented, with a special emphasis on the former. The Junction Riemann Problem is also introduced in Section 3. Section 4 contains a description of the test cases and an analysis of the results obtained. Finally, the conclusions are drawn in Section 5.

2. Mathematical Models

2.1. One-Dimensional Shallow Water Equations

The one-dimensional shallow water equations are given by a system of partial differential equations derived from mass and momentum conservation laws. Assuming a rectangular channel of constant width B, the equations in conservative form are given by

$$\frac{\partial \mathbf{U}(x,t)}{\partial t} + \frac{\partial \mathbf{F}(x,t)}{\partial x} = \mathbf{S}(x,\mathbf{U}). \tag{1}$$

The vector of conserved variables $\mathbf{U}$ and the vector of fluxes both depend on space and time, and are given by

$$\mathbf{U} = \begin{pmatrix} A \\ Q \end{pmatrix}, \qquad \mathbf{F} = \begin{pmatrix} Q \\ \frac{Q^2}{A} + \frac{1}{2}gh^2 \end{pmatrix}, \tag{2}$$

where A is the cross-sectional wetted area, Q is the total discharge, h is the water depth, computed as $h = A/B$, and g is the acceleration due to gravity. The source term accounts for mass and momentum sources and sinks, of which we will only consider the latter, and is given by

$$\mathbf{S} = \begin{pmatrix} 0 \\ \mathcal{T}(\mathbf{U}) \end{pmatrix} = \begin{pmatrix} 0 \\ gA\left(S_o - S_f\right) \end{pmatrix}, \tag{3}$$

where $S_o = -\partial z_b/\partial x$ is the bed slope term and S_f is the friction slope term. In this case, we will assume frictionless channels to obtain a better understanding of the behavior of the method hereby presented.

2.2. Two-Dimensional Shallow Water Equations

The two-dimensional shallow water equations are given by a similar system of partial differential equations:

$$\frac{\partial \mathbf{U}(x,y,t)}{\partial t} + \frac{\partial \mathbf{F}(x,y,t)}{\partial x} + \frac{\partial \mathbf{G}(x,y,t)}{\partial y} = \mathbf{S}(x,y,\mathbf{U}). \tag{4}$$

The vector of conserved variables $\mathbf{U}$ and the vector of fluxes depend on space and time, and are given by

$$\mathbf{U} = \begin{pmatrix} h \\ hu \\ hv \end{pmatrix}, \qquad \mathbf{F} = \begin{pmatrix} hu \\ hu^2 + \frac{1}{2}gh^2 \\ huv \end{pmatrix}, \qquad \mathbf{G} = \begin{pmatrix} hv \\ huv \\ hv^2 + \frac{1}{2}gh^2 \end{pmatrix}, \tag{5}$$

where the velocity vector is split in two components: u along the x direction and v along the y direction. The source term accounts for sinks and sources of mass and momentum, of which only the latter are present:

$$\mathbf{S} = \begin{pmatrix} 0 \\ \mathcal{T}_x(\mathbf{U}) \\ \mathcal{T}_y(\mathbf{U}) \end{pmatrix} = \begin{pmatrix} 0 \\ gh\left(S_{ox} - S_{fx}\right) \\ gh\left(S_{oy} - S_{fy}\right) \end{pmatrix}, \tag{6}$$

where the bed slope term is calculated in each direction

$$S_{ox} = -\frac{\partial z_b}{\partial x}, \qquad S_{oy} = -\frac{\partial z_b}{\partial y}. \tag{7}$$

Again, no friction is considered in this case.

3. Numerical Methods

The numerical model used in both domains is a first-order finite volume scheme. In general, the system of differential equations can be written in integral form over an arbitrary control volume Ω

$$\frac{\partial}{\partial t}\int_\Omega \mathbf{U} d\Omega + \int_\Omega \left(\frac{\partial \mathbf{F}}{\partial x} + \frac{\partial \mathbf{G}}{\partial y}\right) d\Omega = \int_\Omega \mathbf{S} d\Omega, \tag{8}$$

and by using the Gauss–Ostrogrdsky theorem

$$\frac{\partial}{\partial t}\int_{\Omega}\mathbf{U}d\Omega+\oint_{\Omega}\left(\mathbf{F}n_x+\mathbf{G}n_y\right)d\Omega=\int_{\Omega}\mathbf{S}d\Omega, \tag{9}$$

where n_x and n_y are Cartesian components of the unitary outward pointing vector $\mathbf{n}_\Omega$ of the surface surrounding cell Ω.

3.1. One-Dimensional Numerical Method

Equation (9) can be particularized in the case of a one-dimensional domain where a single cell i is defined by its left and right walls $\Omega=[x_L,x_R]$. By also choosing an arbitrary discretization of time in time-steps $\Delta t=t^{n+1}-t^n$, an average value of vector $\mathbf{U}$ in the cell can be found:

$$\mathbf{U}_i^{n+1}=\left(x_R\mathbf{U}(x_R,t^n)-x_L\mathbf{U}(x_L,t^n)\right)-\left(\mathbf{F}(x_R,t)-\mathbf{F}(x_L,t)\right)\Delta t+\int_{t^n}^{t^{n+1}}\int_{x_L}^{x_R}\mathbf{S}dxdt. \tag{10}$$

It is important to note that integration, or linearization, of the source term can be carried out in different manners. In this case, in accordance with the previous literature [27] the bed level source term is computed at the inter-cell walls and introduced into the numerical flux.

$$\hat{\mathbf{U}}_i^{n+1}=\mathbf{U}_i^n-\frac{\Delta t}{\Delta x}\left(\mathbf{F}^-_{i+\frac{1}{2}}-\mathbf{F}^+_{i-\frac{1}{2}}\right) \tag{11}$$

where $\mathbf{F}^{\pm}_{i+\frac{1}{2}}$ represents the numerical flux at the inter-cell wall labeled $i+\frac{1}{2}$ between cells i and $i+1$, which includes the contribution of the source term.

Thus, to compute the conserved variables at the next step, the source term needs to be discretized, and the fluxes need to be found at the cell walls. First, ignoring the linearization of the source term, Equation (1) can be written in non-conservative form

$$\frac{\partial\mathbf{U}(x,t)}{\partial t}+\mathbf{J}(\mathbf{U})\frac{d\mathbf{U}(x,t)}{dx}=\mathbf{S}(x,\mathbf{U}), \tag{12}$$

through the Jacobian matrix $\mathbf{J}(\mathbf{U})$:

$$\mathbf{J}(\mathbf{U})=\begin{pmatrix}0 & 1\\ c^2-u^2 & 2u\end{pmatrix}, \tag{13}$$

where $u=Q/A$ is the flow velocity in the x direction and c is the celerity of the surface waves, defined as $c=\sqrt{gh}$. The hyperbolic property of the convective part is confirmed by the two real eigenvalues:

$$\lambda_1=u-c,\qquad \lambda_2=u+c. \tag{14}$$

If λ_1 and λ_2 have different signs, the regime is said to be subcritical, as the Froude number fulfills $\mathrm{Fr}=u/c<1$. If λ_1 and λ_2 are both positive or negative, then the regime is said to be supercritical and $\mathrm{Fr}>1$. The point at which $u=c$ and $\mathrm{Fr}=1$ is the critical point and is very relevant to define flow transitions and hydraulic jumps.

Additionally, eigenvectors $\mathbf{e}^k$ can be constructed from the eigenvalues:

$$\mathbf{e}^1=\begin{pmatrix}1\\ \lambda_1\end{pmatrix},\qquad \mathbf{e}^2=\begin{pmatrix}1\\ \lambda_2\end{pmatrix}, \tag{15}$$

which can then be organized into the matrix $\mathbf{P}=(\mathbf{e}^1,\mathbf{e}^2)$ to diagonalize the Jacobian. In this way, the Roe scheme is used in order to compute the fluxes at the walls in spite of the non-linearity of the Jacobian matrix by expressing the difference of the conserved variables across the cell walls as the sum of waves associated with the averaged eigenvectors:

$$\delta \mathbf{U}_{i+\frac{1}{2}} = \sum_{m=1}^{2} \left(\tilde{\alpha}_m \mathbf{e}_m\right)_{i+\frac{1}{2}} \tag{16}$$

while the inter-cell numerical fluxes can be written as

$$\mathbf{F}^{-}_{i+\frac{1}{2}} = \mathbf{F}_{i+1} - \sum_{m \mid \tilde{\lambda}_m < 0} \left(\tilde{\gamma}_m \mathbf{e}_m\right)_{i+\frac{1}{2}}, \qquad \mathbf{F}^{+}_{i-\frac{1}{2}} = \mathbf{F}_{i} + \sum_{m \mid \tilde{\lambda}_m > 0} \left(\tilde{\gamma}_m \mathbf{e}_m\right)_{i-\frac{1}{2}}, \tag{17}$$

where γ summarizes the contribution of each wave to the fluxes and the tilde signifies the averaged value at the cell wall:

$$\tilde{\gamma}_{m,i+\frac{1}{2}} = \left(\tilde{\lambda}\tilde{\alpha} - \tilde{\beta}\right)_{m,i+\frac{1}{2}}. \tag{18}$$

According to the literature [27], these averaged values are chosen to be

$$\tilde{\lambda} = \tilde{u} \pm \tilde{c}, \qquad \tilde{c}_{i+\frac{1}{2}} = \sqrt{g\left(\frac{A_i}{B_i} + \frac{A_{i+1}}{B_{i+1}}\right)}, \qquad \tilde{u}_{i+\frac{1}{2}} = \frac{\sqrt{A_i}u_i + \sqrt{A_{i+1}}u_{i+1}}{\sqrt{A_i} + \sqrt{A_{i+1}}} \tag{19}$$

to compute

$$\tilde{\alpha}_{1,i+\frac{1}{2}} = \frac{\tilde{\lambda}_2 \delta A - \delta Q}{2\tilde{c}}, \qquad \tilde{\alpha}_{2,i+\frac{1}{2}} = \frac{-\tilde{\lambda}_1 \delta A + \delta Q}{2\tilde{c}} \tag{20}$$

and the source term contribution:

$$\tilde{\beta}_{1,i+\frac{1}{2}} = -\tilde{\beta}_{2,i+\frac{1}{2}} = \left(\frac{\tilde{S}}{2\tilde{c}}\right)_{i+\frac{1}{2}}. \tag{21}$$

It is convenient to express the effect of inter-cell fluxes using fluctuations $\mathbf{\Delta M}^{\pm}_{i+\frac{1}{2}}$:

$$\mathbf{\Delta M}^{-}_{i+\frac{1}{2}} = \left(\sum_{m \mid \tilde{\lambda}_m < 0} \tilde{\gamma}_m \mathbf{e}_m\right)_{i+\frac{1}{2}}, \qquad \mathbf{\Delta M}^{+}_{i-\frac{1}{2}} = \left(\sum_{m \mid \tilde{\lambda}_m > 0} \tilde{\gamma}_m \mathbf{e}_m\right)_{i-\frac{1}{2}} \tag{22}$$

$$\hat{\mathbf{U}}^{n+1}_i - \mathbf{U}^n_i = \frac{\Delta t}{\Delta x}\left(\mathbf{\Delta M}^{-}_{i+\frac{1}{2}} + \mathbf{\Delta M}^{+}_{i-\frac{1}{2}}\right). \tag{23}$$

Integration of the bed slope term is carried out ensuring the conservation of hydraulic energy in most situations by averaging two different formulations of the discretization [27]. If smooth variation of the variables is assumed, the thrust exerted by changes in the bed can be written in terms of hydrostatic pressure:

$$\left(S^a_o\right)_{i+\frac{1}{2}} = -g\left(\tilde{A}\delta(h+z)\right)_{i+\frac{1}{2}} + \left(\tilde{c}^2 \delta A\right)_{i+\frac{1}{2}}, \tag{24}$$

where $\tilde{A}_{i+\frac{1}{2}}$ and $\tilde{c}_{i+\frac{1}{2}}$ are the Roe-averaged wetted area and wave celerity of the two neighboring cells and $\delta d = (z+h)_{i+1} - (z+h)_i$ is the difference in level of each cell. A suitable alternative if the bed level function includes discontinuities is the integral formulation, obtained by integrating the thrust along the z axis taking into account the relative height of water level and bed at each side of the discontinuity.

$$\left(S^b_o\right)_{i+\frac{1}{2}} = -gA_j\delta(h+z) + \tilde{c}^2\delta A, \tag{25}$$

where index j depends upon the orientation of the discontinuity:

$$A_j = \begin{cases} A_i & \text{if } A_i \leq A_{i+1} \\ A_{i+1} & \text{if } A_i > A_{i+1} \end{cases}. \tag{26}$$

Hence, the energy-conserving source term discretization is formulated as a weighted average:

$$S_o^c = (1 - \mathcal{A})S_o^a + \mathcal{A}S_o^b, \tag{27}$$

where the parameter $\mathcal{A}$ is found assuming conservation of the hydraulic energy

$$H = h + z + \frac{u^2}{2g} \tag{28}$$

and can be written as

$$\mathcal{A}_{i+\frac{1}{2}} = \left(\frac{\delta\left(Q^2/A\right) - \frac{1}{2}\tilde{A}\delta\left(Q^2/A^2\right)}{S_o^b - S_o^a} \right)_{i+\frac{1}{2}}, \tag{29}$$

and is typically bounded by $0 \leq \mathcal{A} \leq 1$. If friction is not considered, it is a well-known result [24] that energy is conserved in most stationary cases, except when there is a hydraulic jump. This structure, comprised of static discontinuity in water surface elevation, appears when a supercritical flow is forcibly decelerated by a downstream condition. Hence, $\mathcal{A}_{i+\frac{1}{2}} = 1$ is locally imposed when $\mathrm{Fr}_i > 1$ and $\mathrm{Fr}_{i+1} < 1$, assuming positive flow velocity.

The time-step Δt in Equations (11) and (23) is variable at each iteration, limited by cell size and the approximate velocity of the waves $\tilde{\lambda}$:

$$\Delta t = \mathrm{CFL} \min_{i,m} \left\{ \frac{\Delta x}{|\tilde{\lambda}_m|_i} \right\} \tag{30}$$

where CFL is the Courant–Friedrich–Lewy number that for this scheme must be less than 1 in order to ensure stability.

3.2. Junction Riemann Problem

The point where 1D channels meet is a junction or confluence, and the cells adjacent to it, the terminal cells, must be solved in a special way. The method proposed in this paper involves treating the junction as an internal boundary condition between the terminal cells, finding the inter-cell fluxes in an alternative way. If an arbitrary junction connects N_c channels, there will be N_c terminal cells, which can be separated into *parents* and *children* according to their relative position to the junction with respect the absolute x-axis. Hence, the orientation of channel k, comprising N_k total cells, will be given by its parameter η_k, defined as follows:

$$\eta_k = \hat{\mathbf{n}}_k \cdot \hat{\mathbf{x}} = \begin{cases} 1 & \text{if } \; i_k = N_k \\ -1 & \text{if } \; i_k = 1 \end{cases}, \tag{31}$$

where $\hat{\mathbf{n}}_k$ is the unit vector pointing from the channel towards the junction and $\hat{\mathbf{x}}_k$ is the unit vector in the x-axis. Thus, it is possible to distinguish when flow is entering ($\eta_k u_k^n < 0$) or leaving ($\eta_k u_k^n > 0$) the channel regardless of whether the terminal cell is located at the beginning or end of the channel. Additionally, the channel Speed Index (SI) is defined as a signed extension to the Froude number

$$\mathrm{SI}_{gk}^n = \eta_k \mathrm{Fr}_k^n, \tag{32}$$

so it contains information on both the flow regime and its direction. The actualization of terminal cell i_k of channel k is a modification of Equation (51):

$$\mathbf{U}_{i_k}^{n+1} = \begin{cases} \mathbf{U}_{i_k}^{n} - \frac{\Delta t}{\Delta x}\left(\mathbf{F}^{-}_{i_k+\frac{1}{2}} - \mathbf{F}^{\star}_{k}\right) & \text{if} \quad \eta_k = -1 \\ \mathbf{U}_{i_k}^{n} - \frac{\Delta t}{\Delta x}\left(\mathbf{F}^{\star}_{k} - \mathbf{F}^{+}_{i_k-\frac{1}{2}}\right) & \text{if} \quad \eta_k = 1 \end{cases}, \tag{33}$$

which includes contributions from both its cell walls, of which one is computed regularly through the linearized flux, while the other is the exact flux through the wall associated with the junction. Figure 1 shows a schematic representation of a three-channel junction, with two parents ($\eta_1 = \eta_3 = 1$) and one child ($\eta_2 = -1$). Terminal cells, in a darker tone, must be computed using Equation (33), where the special flux $F_k^\star$ is associated with the junction walls in red. Rather than using an approximation, since a network of channels will contain many more inter-cell walls than junctions, the latter will be solved through an iterative method that calculates the exact values of the solution to the Riemann problem at each junction wall.

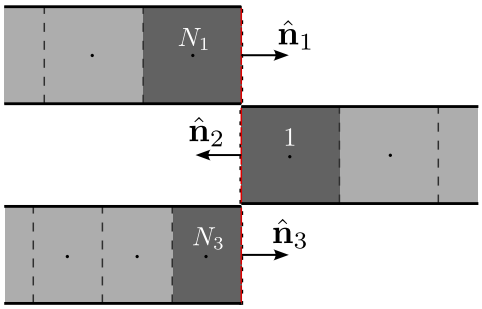

Figure 1. Schematic representation of a junction of three channels.

The Junction Riemann Problem is the set of N_c initial value problems (IVPs),

$$\frac{\partial \mathbf{U}_k(x,t)}{\partial t} + \frac{\partial \mathbf{F}_k(x,t)}{\partial x} = \mathbf{S}_k(x, \mathbf{U}_k), \qquad \mathbf{U}_k(x,0) = \mathbf{U}_k^n, \tag{34}$$

where $k = 1, \ldots, N_p$, along with N_c coupling conditions:

$$\mathbf{\Phi}(\mathbf{U}_1, \ldots, \mathbf{U}_{N_c}) = 0, \tag{35}$$

related to conservation of mass and, in this case, of energy. This yields a non-linear system of $2N_p$ equations that can be used to solve the $2N_p$ unknowns $\{u_1^\star, \ldots, u_{N_c}^\star, A_1^\star \ldots, A_{N_c}^\star\}$, which can be used to compute the inter-cell fluxes. In the subcritical regime, this system takes the following form:

$$\begin{cases} u_1^\star - u_1^n + \eta_1 \mathcal{B}_1 & = 0 \\ \vdots & \\ u_N^\star - u_N^n + \eta_N \mathcal{B}_N & = 0 \\ \sum_k (\eta_k u_k^\star A_k^\star) & = 0 \\ H_1^\star - H_2^\star & = 0 \\ \vdots & \\ H_1^\star - H_N^\star & = 0 \end{cases}, \tag{36}$$

where $\mathcal{B}_k$ is an auxiliary function that solves the rarefaction or shock wave produced as a solution to the Riemann problem and can be defined as follows:

$$\mathcal{B}_k(x) = \begin{cases} 2\sqrt{\frac{g}{B_k}\left(x - A_k^n\right)} & \text{if} \quad x \leq A_k^n \\ \left(x - A_k^n\right)\sqrt{\frac{g}{2B_k}\left(\frac{x + A_k^n}{A_k^n x}\right)} & \text{if} \quad x > A_k^n \end{cases}. \tag{37}$$

Additionally, the N_c-th equation ensures the conservation of mass in the junction and equations $N_c + 1$ to $2N_c$ represent equality of the hydraulic head energy as defined in Equation (28) in all channels, taking channel 1 as the default reference. This does not mean that the energy of channel 1 is fixed, as $(u_1^\star, A_1^\star)$ can vary. The choice of energy conservation might seem controversial in a junction, where wall and angle effects seem important, and it certainly is in cases such as artificial ditches for irrigation or laboratory-scale channels. However, when the concern is on the large-scale wave propagation or transport phenomena in the whole network, or if walls of the junction have a reduced effect, as in river confluences, energy conservation is acceptable. Nevertheless, there is ample literature presenting other models where loss of energy and momentum due the geometry of the junction is taken into account.

System (36) can be solved by any iterative method suitable for a non-linear system of equations. An example is presented in [9,29] using Picard iterations, where a tentative solution $\left(u_k^\star, A_k^\star\right)^m$ is taken to the next iteration $m + 1$ by means of inverting the Jacobian of the error vector.

This methodology is well known has been used in the past to solve networks of channels with one important limitation: the method fails for supercritical flows and even for relatively fast subcritcal flows (Fr > 0.35). This is due to the fact that the solution to each Riemann problem is performed under the assumption that only one wave is propagating into the channel domain from the junction, which is not true in the subcritical regime. Indeed, an out-flowing channel in the supercritical regime (SI > 0) does not fall under this assumption, given that the two waves forming the solution of the RP are at the exterior side of the wall.

In order to extend this method to all regimes, a series of modifications must be introduced, the details of which can be found in [29]. These take the form of a set of coefficients $\{\mathcal{D}_k, \mathcal{R}_k, \mathcal{T}_k, \mathcal{L}_k, \mathcal{Q}_k\}$ that take values 1 or 0 at each step m of the iterative process. The coefficient $\mathcal{D}_k$ is defined as

$$\mathcal{D}_k{}^m = \begin{cases} 0 & \text{if} \quad \text{SI}^n \geq 1 \text{ and, } \eta_k\left(Q_k^\star - Q_k^n\right) > 0 \text{ or } \left(A_k^\star - A_k^n\right) < 0 \\ 0 & \text{if} \quad \text{SI}^n \geq 1 \text{ and } -\eta_k \mathcal{S}_k^{\star,m} < 0 \\ 1 & \text{otherwise} \end{cases}, \tag{38}$$

where $\mathcal{S}_k^{\star,m}$ is the speed of a tentative shock-type solution at iterative step m at channel k, and is computed as follows:

$$\mathcal{S}_k^{\star,m} = \left(\frac{Q_k^\star - Q_k^n}{A_k^\star - A_k^n}\right)^m. \tag{39}$$

Then, $\mathcal{D}_k = 0$ occurs only in cases where the cell is initially in the supercritical regime and is tentatively being accelerated further, or if the tentative solution is a shock wave moving towards the junction.

Coefficients $\mathcal{T}_k$ and $\mathcal{R}_k$ are used to ensure that a rarefaction-type solution cannot be accelerated further towards a junction,

$$\mathcal{R}_k{}^m = \begin{cases} 1 & \text{if} \quad \text{SI}^{\star,m} < 1 \text{ and } \text{SI}^{\star,m+1} > 1 \text{ and } \left(A_k^{\star,m} - A_k^n\right) < 0 \\ 0 & \text{otherwise} \end{cases}, \tag{40}$$

and

$$\mathcal{T}_k{}^m = 1 - \mathcal{R}_k{}^m. \tag{41}$$

In this way, $\mathcal{R}_k$ takes a value of 1 right at the iteration when a tentative rarefaction-type solution $(A_k^{\star,m} - A_k^n)$ would enter the supercritical regime. Otherwise, $\mathcal{R}_k = 0$ and then $\mathcal{T}_k = 1$, the normal behavior.

The remaining coefficients, $\mathcal{L}_k$ and $\mathcal{Q}_k$, play their part in ensuring that channels of the junction whose behavior is affected by the previous coefficients cannot take part in energy conservation. If, by chance, the default reference channel for energy continuity is locked by $\mathcal{D}_k = 0$ or $\mathcal{T}_k = 0$, it cannot take part in energy conservation and thus another reference must be found. Hence, $\mathcal{L}_k$ is defined as

$$\mathcal{L}_k = \begin{cases} 1 & \text{if} \quad k = k_{\mathcal{L}} \geq 1 \\ 0 & \text{otherwise} \end{cases}, \qquad k_{\mathcal{L}} = \min\{k \ : \ \mathcal{T}_k \mathcal{D}_k = 1\}, \tag{42}$$

so it takes a value of 1 only for the first channel that is not locked out of energy conservation, and therefore the reference energy can be defined as follows:

$$H^\star_{ref} = \sum_k \mathcal{L}_k H^\star_k. \tag{43}$$

Once the reference is chosen, every other ineligible channel must be excluded too. This is carried out through the $\mathcal{Q}_k$ coefficient, defined simply as follows:

$$\mathcal{Q}_k = \mathcal{T}_k \mathcal{D}_k (1 - \mathcal{L}_k). \tag{44}$$

By defining these coefficients, system (36) can be rewritten as follows:

$$\begin{cases} \left[u^\bullet_1 - u^n_1 + g_1 \mathcal{B}(A^\star_1)\right]\mathcal{D}_1 & + \left[u^\star_1 - u^n_1\right](1 - \mathcal{D}_1) & = 0 \\ & \vdots & \\ \left[u^\bullet_N - u^n_N + g_N \mathcal{B}(A^\star_N)\right]\mathcal{D}_N & + \left[u^\star_N - u^n_N\right](1 - \mathcal{D}_N) & = 0 \\ \Sigma_k \eta_k \Big(\mathcal{D}_k (A^\star_k u^\bullet_k) & + \mathcal{Q}^n_k (1 - \mathcal{D}_k) \Big) & = 0 \\ \left(H^\star_{ref} - H^\star_2\right)\mathcal{Q}_2 & + \delta A_1 (1 - \mathcal{D}_1)\mathcal{L}_2 + \delta A_2 (1 - \mathcal{D}_2) & = 0 \\ & \vdots & \\ \left(H^\star_{ref} - H^\star_N\right)\mathcal{Q}_N & + \delta A_1 (1 - \mathcal{D}_1)\mathcal{L}_N + \delta A_N (1 - \mathcal{D}_N) & = 0 \end{cases}, \tag{45}$$

where $u^\bullet_k$ allows the velocity to be limited when a critical rarefaction occurs in any channel, and is defined as

$$u^\bullet_k = \eta_k \mathcal{R}_k c^\star_k + \mathcal{T}_k u^\star_k, \tag{46}$$

because SI $= 1$, the critical point, implies that $u = c$. It can be seen that all the equations of the system have two parts. The first deals with all cases where the terminal state is, in principle, not locked by $\mathcal{D}_k = 0$. The second part forces the evolved state to remain unchanged in the cases where the terminal cell cannot be affected due to it fulfilling the conditions of $\mathcal{D}_k = 1$. System (45) is again non-linear, but can be solved iteratively to find the exact solution of the JRP $\{u^\star_1, \ldots, u^\star_{N_c}, A^\star_1 \ldots, A^\star_{N_c}\}$ under all circumstances to compute $F^\star_k$ simply as

$$\mathbf{F}^\star_k = \begin{pmatrix} u^\star_k A^\star_k \\ u^{\star 2}_k A^\star_k + \frac{g A^{\star 2}_k}{2 B^2_k} \end{pmatrix}, \tag{47}$$

which in turn completes the actualization of the terminal cell through Equation (33).

3.3. Two-Dimensional Numerical Method

The numerical method used to solve the 2-dimensional model given by the hyperbolic system (4) is also a first-order finite volume scheme, as laid out in Equation (9). The basic concepts are similar to the 1D scheme presented in this paper, so it will only be summarized

here. Further information can be found in [31]. The Jacobian matrix, defined through the fluxes, is as follows:

$$\mathbf{J} = \frac{\partial \mathbf{F}}{\partial \mathbf{U}} n_x + \frac{\partial \mathbf{G}}{\partial \mathbf{U}} n_y = \begin{pmatrix} 0 & n_x & n_y \\ (c^2 - u^2) n_x - uvn_y & vn_y + 2un_x & un_y \\ (c^2 - v^2) n_y - uvn_x & vn_x & un_x + 2vn_y \end{pmatrix}. \tag{48}$$

Its eigenvalues and eigenvectors can again be found in order to diagonalize the matrix

$$\lambda_1 = \mathbf{u} \cdot \mathbf{n} - c, \qquad \lambda_2 = \mathbf{u} \cdot \mathbf{n}, \qquad \lambda_3 = \mathbf{u} \cdot \mathbf{n} + c, \tag{49}$$

and

$$\mathbf{e}^1 = \begin{pmatrix} 1 \\ u - cn_x \\ v - cn_y \end{pmatrix}, \qquad \mathbf{e}^2 = \begin{pmatrix} 0 \\ -cn_y \\ cn_x \end{pmatrix}, \qquad \mathbf{e}^3 = \begin{pmatrix} 0 \\ u + cn_x \\ v + cn_y \end{pmatrix}. \tag{50}$$

Thus, the expression for the actualization of the 2D cell is analogous to that of the 1D scheme given in Equation (23): each cell i with area Ω_i is updated according to the contribution of each wave m at each of its N_w walls (three for a triangular cell, four for a rectangular cell, etc.) of length l_k:

$$\mathbf{U}_i^{n+1} = \mathbf{U}_i^n - \frac{\Delta t}{\Omega_i} \left(\sum_{k=1}^{N_w} \sum_m (\tilde{\gamma}^m \mathbf{e}^m)_k l_k \right) + \Delta t \begin{pmatrix} 0 \\ \bar{S}_{fx} \\ \bar{S}_{fy} \end{pmatrix}_i, \tag{51}$$

where again $\tilde{\gamma}_k^m$ contains the contributions of the fluxes and source terms:

$$\tilde{\gamma}_k^m = \left(\tilde{\lambda} \tilde{\alpha} - \tilde{\beta} \right)_k^m. \tag{52}$$

To ensure stability, the global time-step Δt is limited, requiring the smallest out of all the meshes to be chosen, defined as:

$$\Delta t = \mathrm{CFL} \min_{k,m} \left\{ \frac{\min \left\{ \frac{\Omega_i}{l_p} \right\}_{p=1,\ldots,N_w}}{|\tilde{\lambda}_m^k|} \right\} \tag{53}$$

where, again, CFL < 1 must hold.

4. Computational Experiments

In this section, the 1D method is tested against a well-established 2D method that is often used to tackle large-scale simulations of free-surface flows through a series of numerical experiments involving transitory flow in junctions. It is worth noting that the reference 2D results have been obtained ad hoc by the authors using energy-balanced methods that can overcome all types of situations in shallow flows, not only under arbitrary geometries, but also independent of the rheological shear stress model selected. Reference [29] presents a series of academic test cases where a specific JRP configurations were solved using the 1D method and compared with the known exact solution. In contrast, the validation here is focused on practical cases.

4.1. Three-Channel Junctions

The first batch of experiments deals with a single junction of three channels, in which all of them are parallel. These types of configurations were proposed in [1] to test their 1D method based on the PSP. In principle, this particular geometry is the closest to the idea

of the junction as a singular point. Figure 2 presents the configurations used in the tests, throughout which the width of parent channel 1 is kept constant at $B = 1$ m and the widths of children channels 2 and 3 are either $0.5B$ or B depending on the case. Initially, the whole domain is set to the following conditions:

$$h(x, 0) = 0.16 \text{ m}, \qquad hu(x, 0) = 0 \text{ m}^2/\text{s}. \tag{54}$$

A discharge over time boundary condition is imposed on the parent channel, given by a Gaussian function

$$q(t) = 0.4e^{-0.5(t-3)^2}, \tag{55}$$

that evolves into a shock as it travels along the parent channel. A free boundary condition is imposed at the end of the children channels, but they are made sufficiently long as to avoid any effect of the outlets. Measurements are taken at positions $P1$, $P2$, and $P3$, all of them 2 m from the junction. In 1D, the measurement is taken directly at the cell. In 2D, however, the average value in the transversal direction is taken to smooth out local fluctuations.

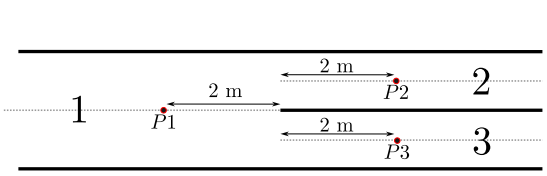

(**a**) Geometry of case 1A

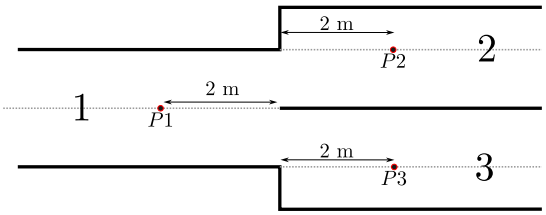

(**b**) Geometry of case 1B

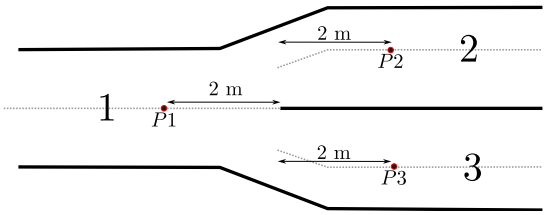

(**c**) Geometry of case 1C

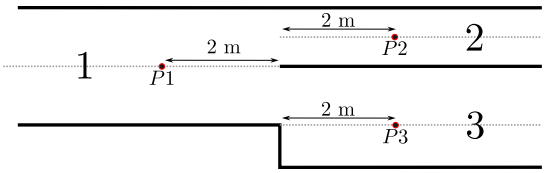

(**d**) Geometry of case 1D

Figure 2. Geometries of 3-channel junctions tested.

Case 1A is the simplest case, where a parent channel seamlessly divides into two children channels of half the width. It is expected that the traveling wave will propagate without any change in shape. The time evolution of depth and the Froude number are pictured in Figure 3, where it can be seen that the coincidence is very good. The Froude numbers reach a peak value of 0.6 approximately, still in the subcritical regime but still relatively high for current methods used to solve junctions.

A snapshot of the channels at $t = 8$ s is shown in Figure 4, when the wave has already passed through the junction. Here, the discrepancies between the methods can be perceived more starkly, with the 1D solution producing a slower-moving wave.

This is due to the difference in propagation in a 1D discretized channel or in a 2D triangular unstructured mesh in a first-order method. To prove that the differences are not introduced by the junction, Figure 5 shows the propagation of the wave in the parent channel before it has reached the confluence. Here, the deformation can already be observed. The shock wave is not as sharp as in the 2D reference solution due to the unstructured mesh. As it propagates down the children channels, the difference in wave speed becomes more pronounced.

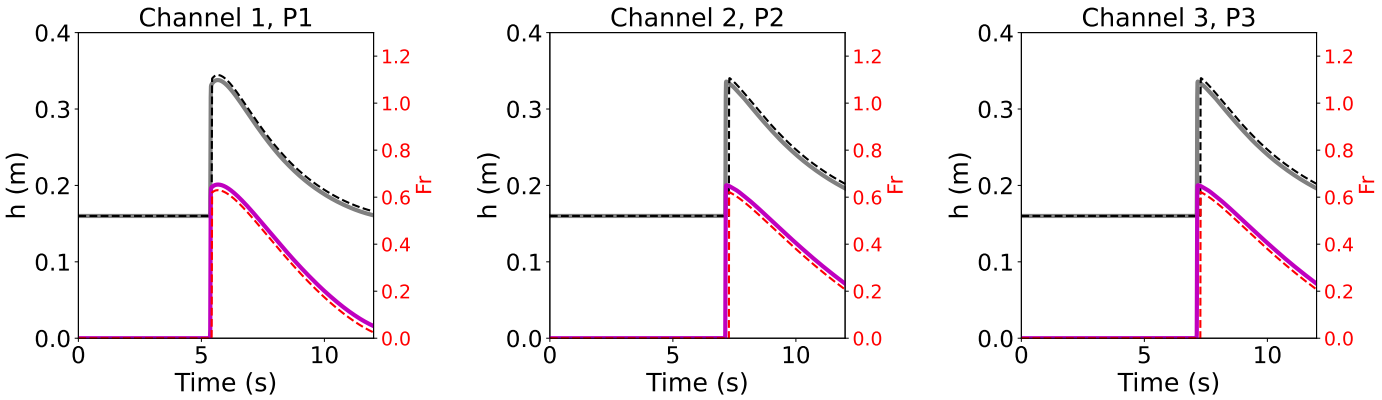

(**a**) Probe 1 (**b**) Probe 2 (**c**) Probe 3

Figure 3. Case 1A. Time evolution at probes $P1$, $P2$, and $P3$. The solid line $(-)$ marks the reference 2D solution, while the dashed line $(--)$ marks the 1D solution. Depth (black) is pictured with reference to the left y-axis while the Froude (red) number is pictured with reference to the right y-axis.

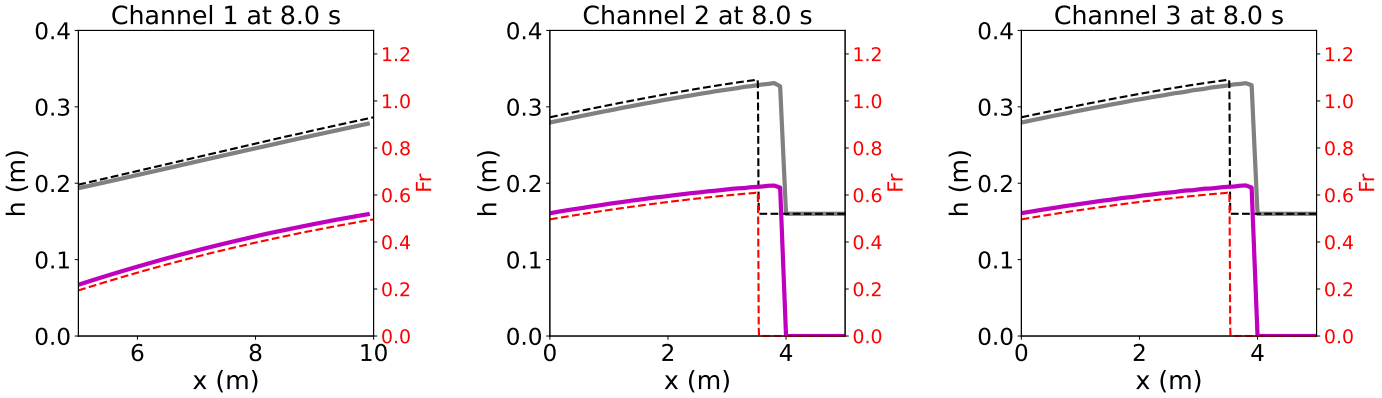

(**a**) Channel 1 (**b**) Channel 2 (**c**) Channel 3

Figure 4. Case 1A. State of the channels at $t = 8$ s. The solid line $(-)$ marks the reference 2D solution, while the dashed line $(--)$ marks the 1D solution. Depth (black) is pictured with reference to the left y-axis while the Froude (red) number is pictured with reference to the right y-axis.

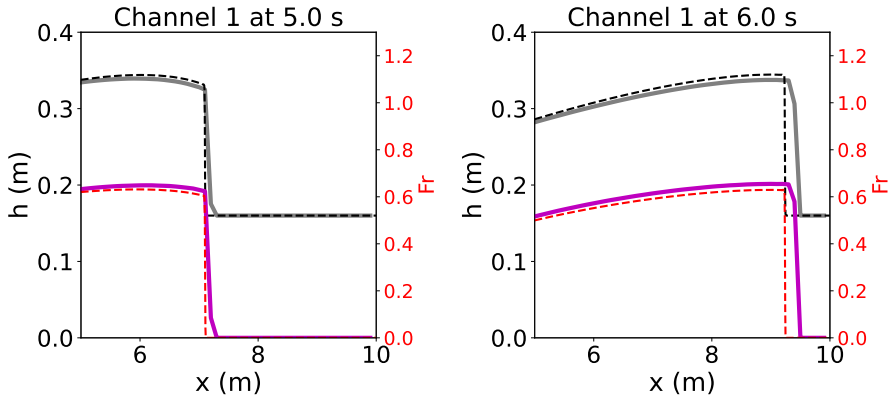

(**a**) Channel 1 at $t = 5$ s. (**b**) Channel 1 at $t = 6$ s.

Figure 5. Case 1A. (**a**): State of channel 1 at $t = 5$ s. (**b**): State of channel 1 at $t = 6$ s. The solid line $(-)$ marks the reference 2D solution, while the dashed line $(--)$ marks the 1D solution. Depth (black) is pictured with reference to the left y-axis while the Froude (red) number is pictured with reference to the right y-axis.

Case 1B includes a sudden expansion of the parent channel into two children channels of the same width right at the junction. By the effect of the width source term, the parent channel will be accelerated, and the wave will be deformed. Again, the time evolution of depth and Froude number at the selected probes is shown in Figure 6. It can be observed that channel 1 is accelerated by the effect of the sudden expansion and a rarefaction propagates upstream, and this behavior is reproduced correctly in 1D. Downstream, the propagation of the shock wave is also well reproduced, albeit with slight delays in its arrival and in its maximum water surface elevation. Figure 7 provides further insight, as it pictures a snapshot of the channels at $t = 8$ s. Upstream, the parent channel is accelerated towards the junction, reaching the critical point exactly there. By the restrictions applied to the method, no further acceleration is allowed, as once the supercritical regime is reached, no perturbations can travel upstream. The reference solution in 2D is also accelerated towards the junction, but it does not quite reach the critical point there. Instead, its Froude number grows continuously until reaching a maximum in the children channels.

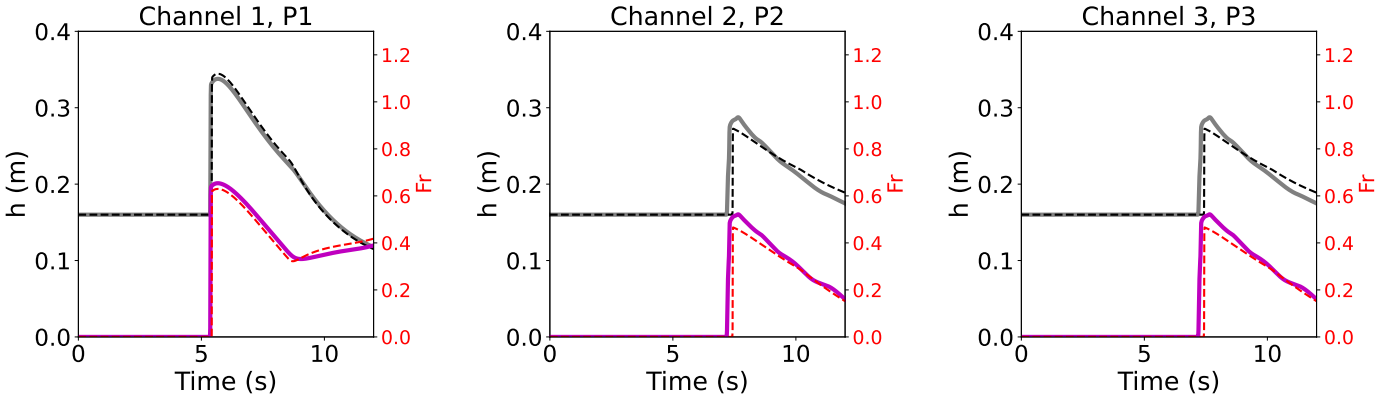

(**a**) Probe 1 (**b**) Probe 2 (**c**) Probe 3

Figure 6. Case 1B. Time evolution at probes $P1$, $P2$, and $P3$. The solid line $(-)$ marks the reference 2D solution, while the dashed line $(--)$ marks the 1D solution. Depth (black) is pictured with reference to the left y-axis while the Froude (red) number is pictured with reference to the right y-axis.

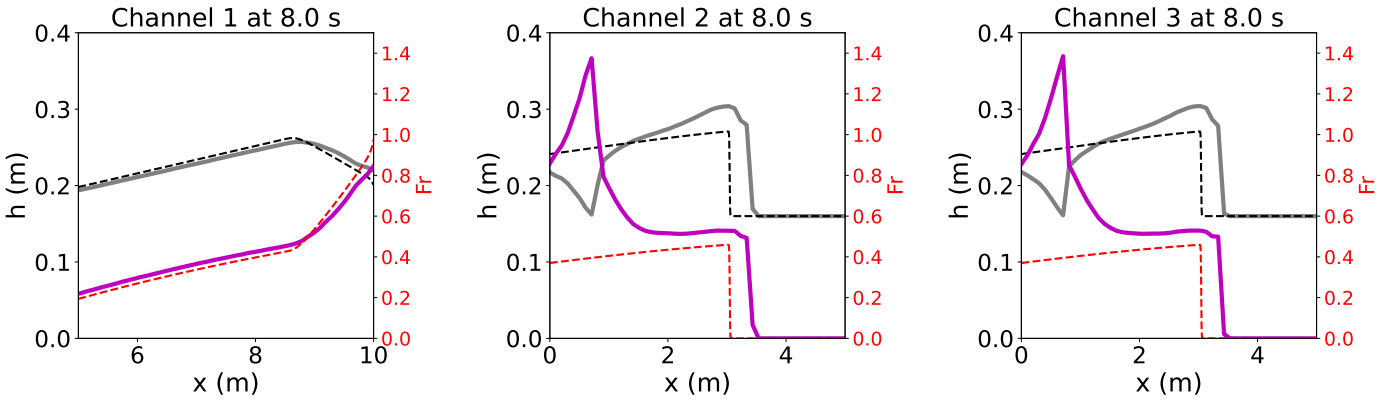

(**a**) Channel 1 at $t = 8$ s. (**b**) Channel 2 at $t = 8$ s. (**c**) Channel 3 at $t = 8$ s.

Figure 7. Case 1B. State of the channels at $t = 8$ s. The solid line $(-)$ marks the reference 2D solution, while the dashed line $(--)$ marks the 1D solution. Depth (black) is pictured with reference to the left y-axis while the Froude (red) number is pictured with reference to the right y-axis.

Case 1C also considers a widening of the channel, but this time the expansion is linear, with the junction placed right at its middle. As a consequence, the acceleration to the supercritical regime occurs at the parent channel, as can be observed in Figures 8 and 9. The dynamics of the waves are correctly reproduced in 1D, both the rarefaction traveling upstream and the shockwave traveling downstream, albeit with the small delay that has been constantly observed. A noteworthy detail is the small bump observed in channels 2 and 3, not present in the 2D reference solution. This is a direct result of the supercritical-to-subcritical transition occurring upstream. To understand this issue, it is worth taking a look at the snapshot of the channels at $t = 11$ s, as pictured in Figure 10 with special attention at the parent channel in the vicinity of the junction.

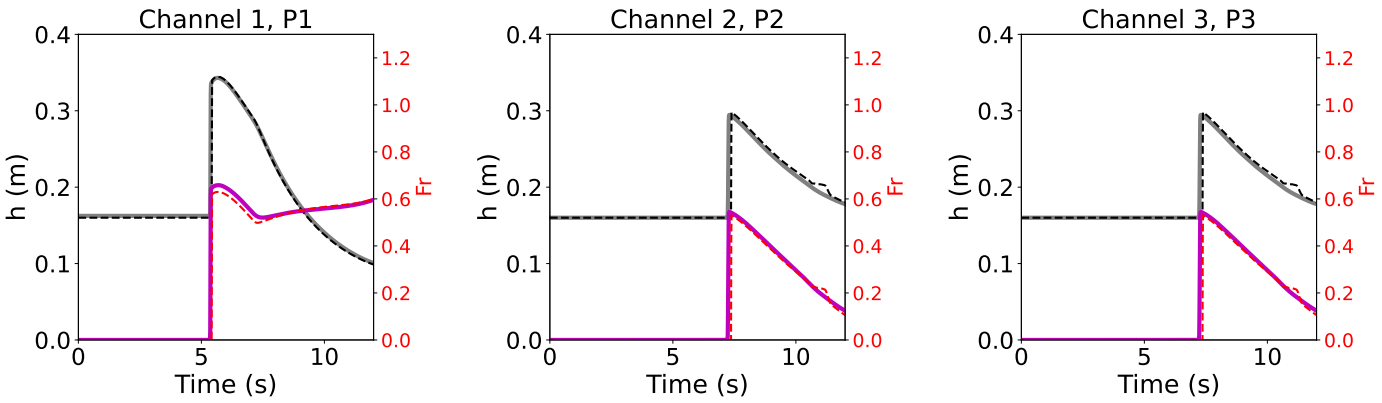

(**a**) Probe 1 (**b**) Probe 2 (**c**) Probe 3

Figure 8. Case 1C. Time evolution at probes $P1$, $P2$, and $P3$. The solid line $(-)$ marks the reference 2D solution, while the dashed line $(--)$ marks the 1D solution. Depth (black) is pictured with reference to the left y-axis while the Froude (red) number is pictured with reference to the right y-axis.

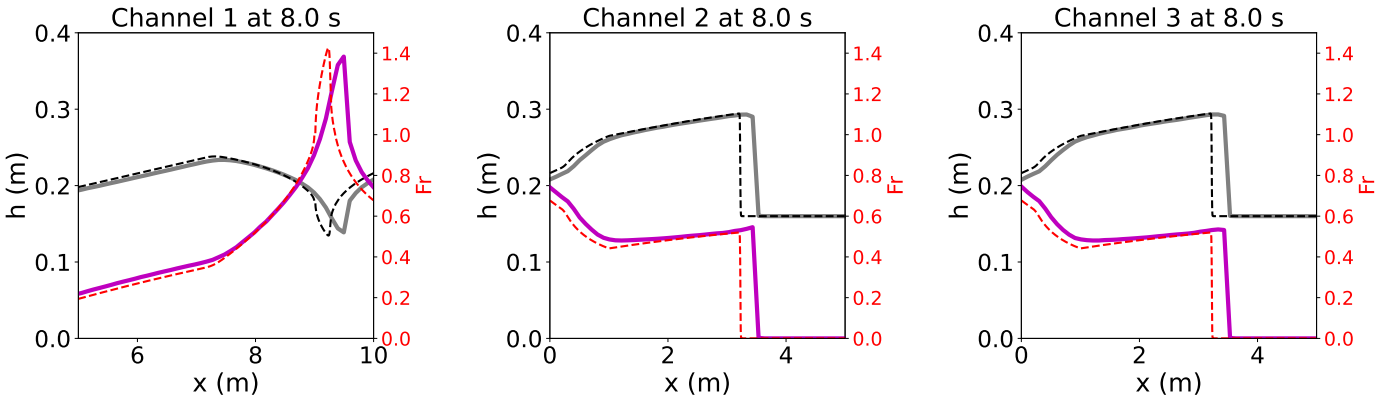

(**a**) Channel 1 at $t = 8$ s. (**b**) Channel 2 at $t = 8$ s. (**c**) Channel 3 at $t = 8$ s.

Figure 9. Case 1C. State of the channels at $t = 8$ s. The solid line $(-)$ marks the reference 2D solution, while the dashed line $(--)$ marks the 1D solution. Depth (black) is pictured with reference to the left y-axis while the Froude (red) number is pictured with reference to the right y-axis.

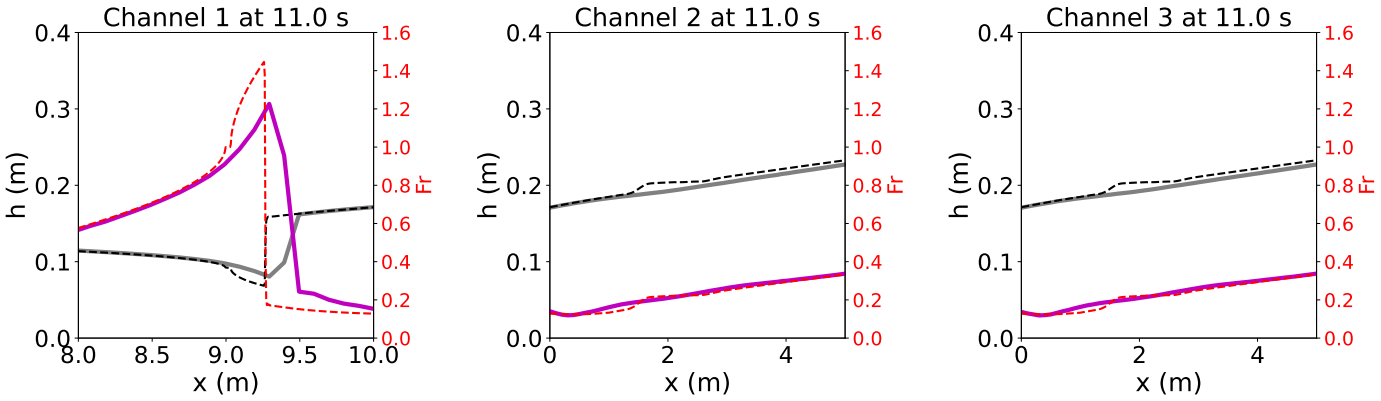

(**a**) Channel 1 at $t = 11$ s. (**b**) Channel 2 at $t = 11$ s. (**c**) Channel 3 at $t = 11$ s.

Figure 10. Case 1C. State of the channels at $t = 11$ s. The solid line $(-)$ marks the reference 2D solution, while the dashed line $(--)$ marks the 1D solution. Depth (black) is pictured with reference to the left y-axis while the Froude (red) number is pictured with reference to the right y-axis.

While it is obvious that the 1D method is unable to exactly reproduce the shape of the 2D reference solution, it is remarkable that it reproduces the hydraulic jump. This is due to the JRP forcing a subcritical solution at the end of the supercritical 1D parent channel. The only possible solution to this configuration is the hydraulic jump pictured in the figure. The bump, or spike, appearing downstream is a known consequence of representing this sharp discontinuities in a finite-volume grid [32]. Regardless of the small bump, the fact that the 1D method can reproduce this feature is a remarkable result that has not been achieved by other methods, as it is a product of combining supercritical and subcritical regimes.

Case 1D is included to test the ability of the method to reproduce an asymmetrical junction. Again, the features of the reference 2D solution are reproduced by the 1D method, as observed in Figures 11 and 12, including the acceleration of the parent channel and its subsequent deceleration. Likewise, the two children channels behave appropriately, with differences more apparent in Figure 12.

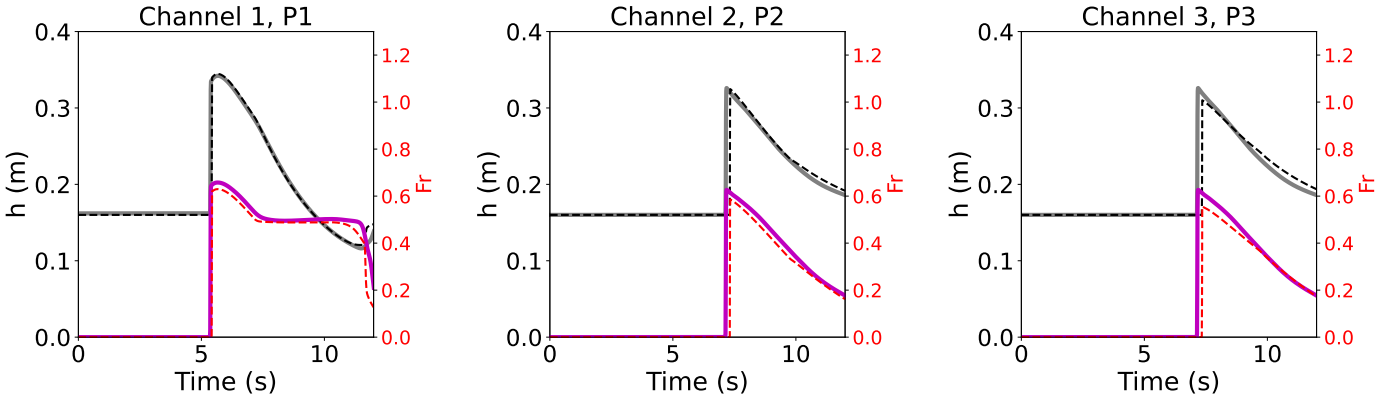

(**a**) Probe 1. (**b**) Probe 2. (**c**) Probe 3.

Figure 11. Case 1D. Time evolution at probes $P1$, $P2$, and $P3$. The solid line $(-)$ marks the reference 2D solution, while the dashed line $(--)$ marks the 1D solution. Depth (black) is pictured with reference to the left y-axis while the Froude (red) number is pictured with reference to the right y-axis.

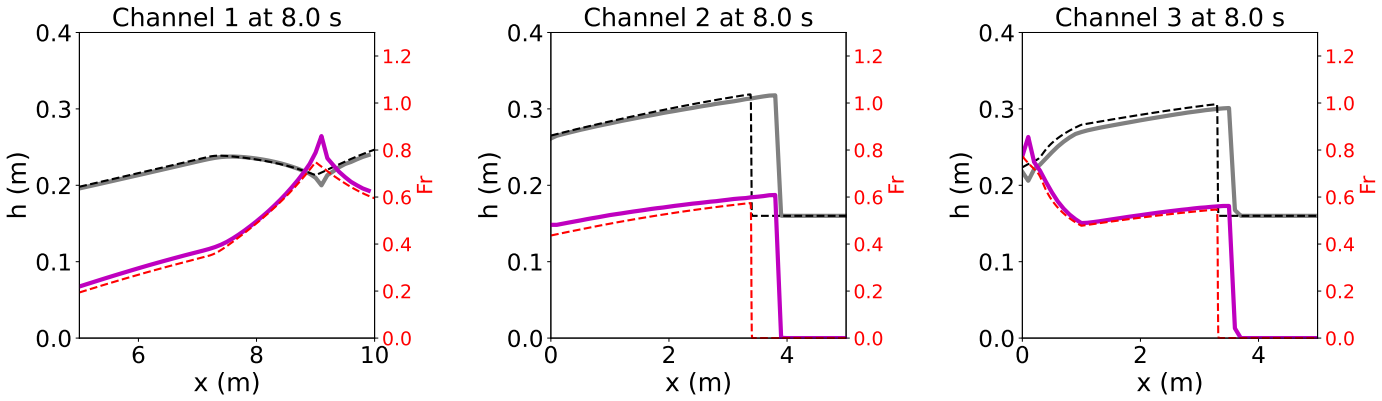

(**a**) Channel 1 at $t = 8$ s. (**b**) Channel 2 at $t = 8$ s. (**c**) Channel 3 at $t = 8$ s.

Figure 12. Case 1D. State of the channels at $t = 8$ s. The solid line $(-)$ marks the reference 2D solution, while the dashed line $(--)$ marks the 1D solution. Depth (black) is pictured with reference to the left y-axis while the Froude (red) number is pictured with reference to the right y-axis.

The results with this basic junction configuration are promising. First, the method is robust and able.

4.2. Large Network

In order to test the capabilities of the model in a complex case, a large network of 24 channels and 16 junctions has been devised, inspired by a similar structure in [1]. The layout of the network in 2D is shown in Figure 13, with a detail of the fine meshing. The whole structure is 500 m long and all channels have a constant width of $B = 5$ m. There is a single inlet at channel 1, with a discharge over time boundary condition, and a single outlet at channel 24, with a free outflow boundary condition. In any case, channel 24 has been made long enough to avoid any effect of the outlet propagating back into the domain.

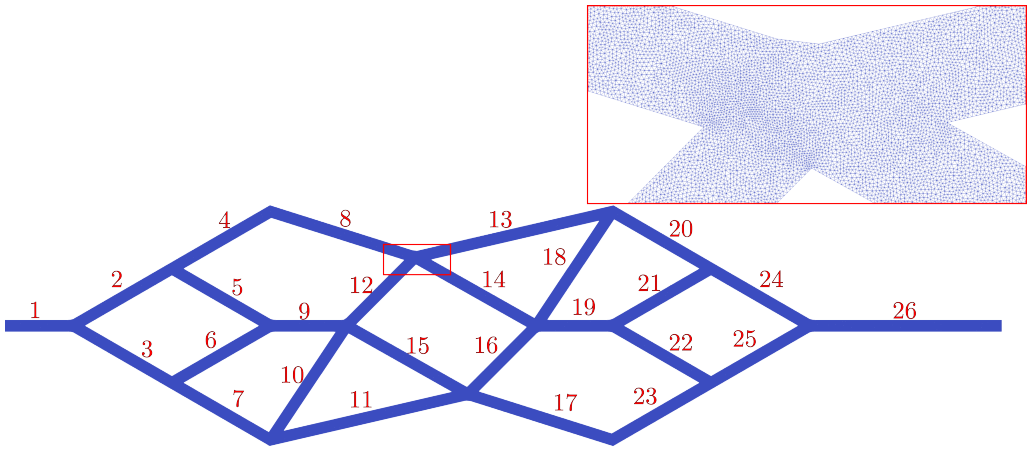

Figure 13. Two-dimensional mesh of the large network, with an example of the fine unstructured triangular cells used.

The boundary condition at channel 1 is given by a Gaussian function

$$q(t) = 4e^{-0.5(t-3)^2}, \tag{56}$$

which, combined with the initial conditions

$$h(x,0) = 0.2\ \text{m}, \qquad hu(x,0) = 0\ \text{m}^2/\text{s}, \tag{57}$$

ensures that the wave arrives at the first junction in the supercritical regime. This test serves to highlight the capabilities of the method, so the 1D solution is not expected to perfectly coincide with the 2D reference.

Indeed, Figure 14 show a collage of time evolution series at the center points of several channels. The 1D solution performs well for the first few channels, but as the wave propagates through the channels the discrepancies grow larger. However, the relative structures of the solutions are kept, meaning that the coupling conditions of the 1D method at the junctions are working correctly. It is then a matter of the propagation along the channels that is causing the delays observed. It is specially remarkable that the solutions at channels 12, 14, 15, and 16 keep a similar pattern, especially in the Froude number, even if displaced and dumped. These channels are located in the center part of the network; thus, they are subject to many oncoming waves and reflections. This is coherent with the observations made in the previous batch of test cases.

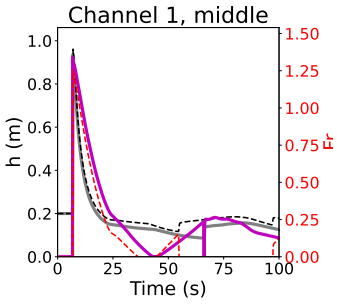

(**a**) Middle point of channel 1.

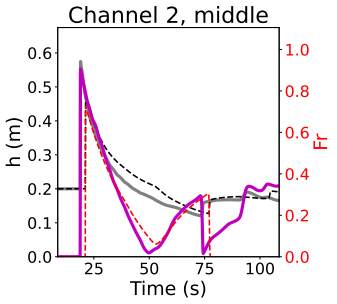

(**b**) Middle point of channel 2.

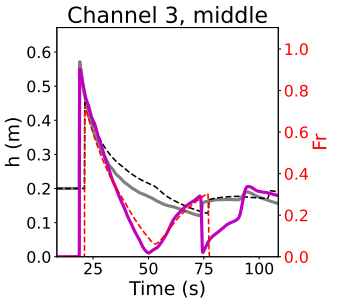

(**c**) Middle point of channel 3.

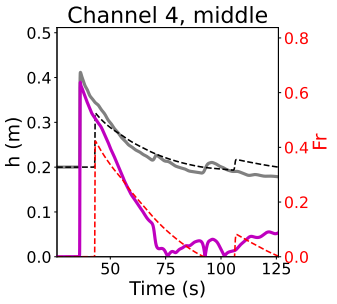

(**d**) Middle point of channel 4.

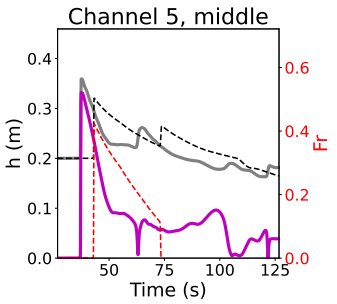

(**e**) Middle point of channel 5.

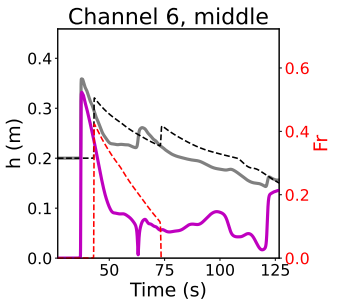

(**f**) Middle point of channel 6.

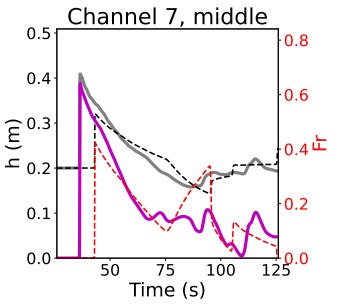

(**g**) Middle point of channel 7.

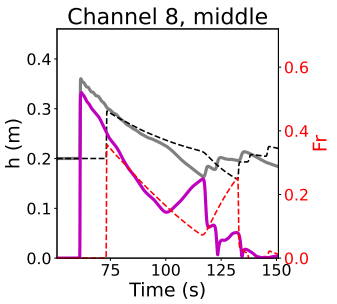

(**h**) Middle point of channel 8.

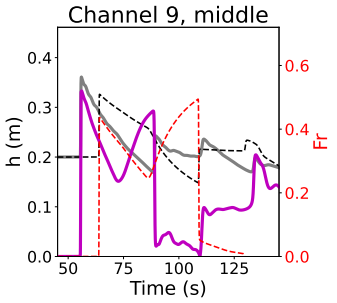

(**i**) Middle point of channel 9.

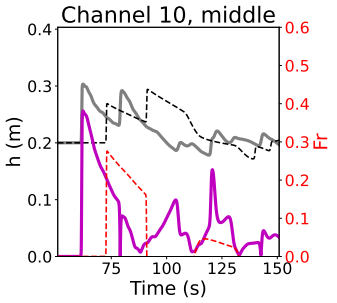

(**j**) Middle point of channel 10.

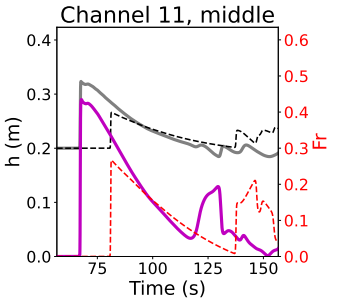

(**k**) Middle point of channel 11.

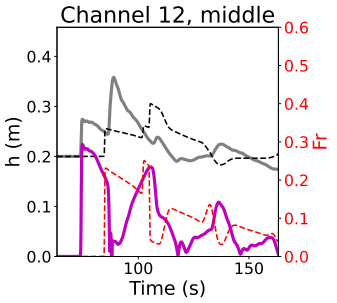

(**l**) Middle point of channel 12.

Figure 14. *Cont.*

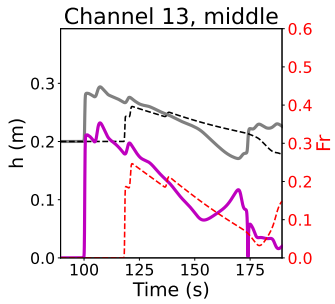

(**m**) Middle point of channel 13.

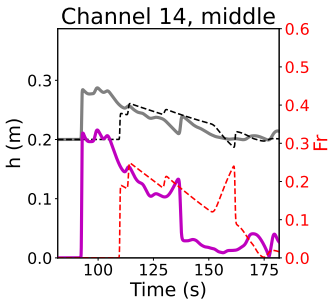

(**n**) Middle point of channel 14.

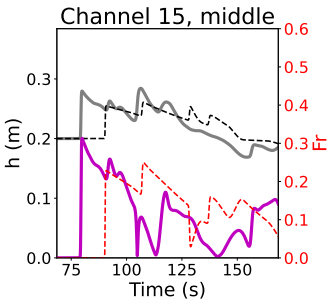

(**o**) Middle point of channel 15.

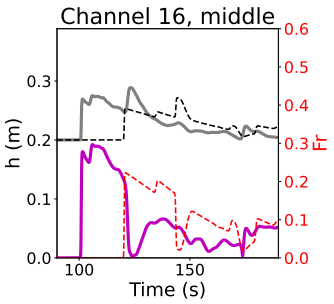

(**p**) Middle point of channel 16.

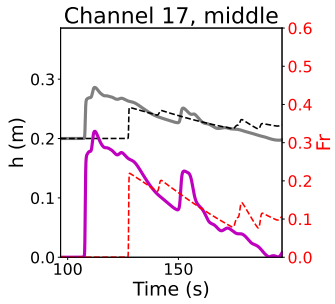

(**q**) Middle point of channel 17.

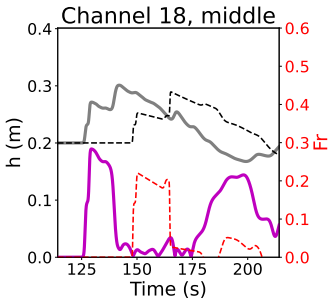

(**r**) Middle point of channel 18.

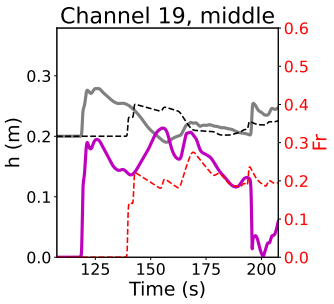

(**s**) Middle point of channel 19.

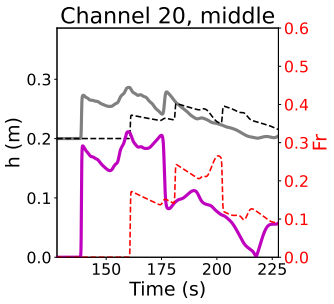

(**t**) Middle point of channel 20.

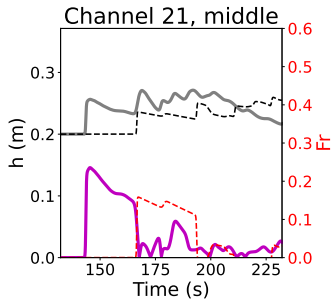

(**u**) Middle point of channel 21.

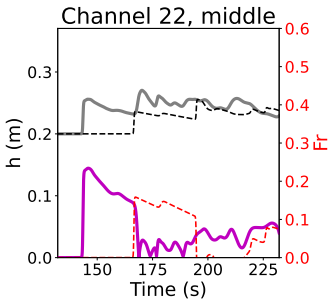

(**v**) Middle point of channel 22.

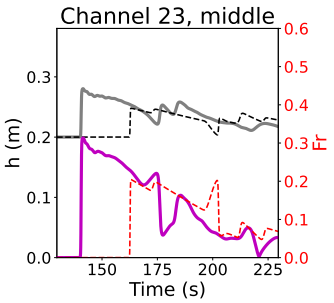

(**w**) Middle point of channel 23.

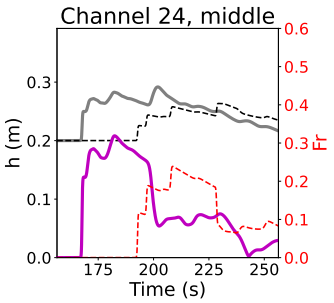

(**x**) Middle point of channel 24.

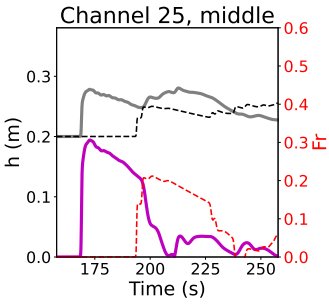

(**y**) Middle point of channel 25.

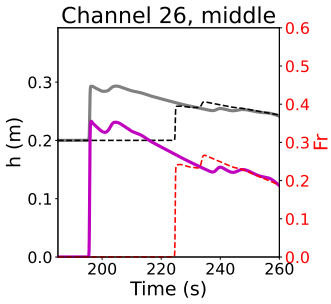

(**z**) Middle point of channel 26.

Figure 14. Time evolution of several probes located at the center of the channels of the large network. The solid line (−) marks the reference 2D solution, while the dashed line (−−) marks the 1D solution. Depth (black) is pictured with reference to the left y-axis while the Froude number (red) is pictured with reference to the right y-axis.

Likewise, the probe at Channel 26, the last channel of the network, shows that after going through 16 junctions, the wave This is a testament to the method's robustness.

5. Conclusions

This work shows that a fully one-dimensional formulation of channel networks that contemplates transitory states and supercritical transitions is possible through the Junction Riemann Problem and conservation of mass and energy.

By including some limiting coefficients in the coupling condition at the junction, the different combinations of regimes can be managed to achieve a coherent solution. This translates into a robust method that can handle complex networks with multiple junctions of several channels, independently of their geometry. Of course, given that energy conservation is assumed, the method will not take into account energy loss due to friction and reflections at the junction walls. This limitation can be addressed in future works. For now, the robustness of the method in the complex configurations tested is a promising result.

Given the computational efficiency of 1D methods as opposed to 2D, it can be concluded that this formulation of the JRP makes pure 1D methods a viable option for solving networks of channels independently of the regime of the flow.

Author Contributions: Conceptualization, J.M. (Javier Murillo) and P.G.-N.; methodology, J.M. (Juan Mairal) and J.M. (Javier Murillo); software, J.M. (Juan Mairal); validation, J.M. (Juan Mairal); formal analysis, J.M. (Juan Mairal); writing—original draft preparation, J.M. (Juan Mairal); writing—review and editing, J.M. (Juan Mairal), J.M. (Javier Murillo), and P.G.-N.; visualization, J.M. (Juan Mairal); supervision, J.M. (Javier Murillo) and P.G.-N.; project administration, P.G.-N.; funding acquisition, P.G.-N. All authors have read and agreed to the published version of the manuscript.

Funding: This work was supported by project PID2022-137334NB-I00 funded by MCIN/AEI/10.13039/501100011033 and by "ERDF/EU" of the Spanish Ministry of Science and Innovation and the European Regional Development Fund. It is also partially funded by the Government of Aragón, through the research grant T32_23R Fluid Dynamics Technologies.The authors belong to and are supported by the Aragón Institute of Engineering Research (I3A) of the University of Zaragoza. The first author is funded by the Spanish Ministry of Universities by grant FPU21/02876.

Data Availability Statement: The raw data supporting the conclusions of this article will be made available by the authors on request.

Conflicts of Interest: The authors declare no conflicts of interest. The funders had no role in the design of the study; in the collection, analyses, or interpretation of data; in the writing of the manuscript; or in the decision to publish the results

References

1. Bellamoli, F.; Müller, L.O.; Toro, E.F. A numerical method for junctions in networks of shallow-water channels. *Appl. Math. Comput.* **2018**, *337*, 190–213. [CrossRef]
2. Herty, M.; Izem, N.; Seaid, M. Fast and accurate simulations of shallow water equations in large networks. *Comput. Math. Appl.* **2019**, *78*, 2107–2126. [CrossRef]
3. Bales, P.; Kolb, O.; Lang, J. Hierarchical modelling and model adaptivity for gas flow on networks. In Proceedings of the Computational Science–ICCS 2009: 9th International Conference, Baton Rouge, LA, USA, 25–27 May 2009; Proceedings, Part I 9; Springer: Berlin/Heidelberg, Germany, 2009; pp. 337–346.
4. Bermudez, A.; López, X.; Vázquez-Cendón, M.E. Numerical solution of non-isothermal non-adiabatic flow of real gases in pipelines. *J. Comput. Phys.* **2016**, *323*, 126–148. [CrossRef]
5. Bermúdez, A.; López, X.; Vázquez-Cendón, M.E. Treating network junctions in finite volume solution of transient gas flow models. *J. Comput. Phys.* **2017**, *344*, 187–209. [CrossRef]
6. Quarteroni, A.; Tuveri, M.; Veneziani, A. Computational vascular fluid dynamics: Problems, models and methods. *Comput. Vis. Sci.* **2000**, *2*, 163–197. [CrossRef]

7. Müller, L.O.; Blanco, P.J. A high order approximation of hyperbolic conservation laws in networks: Application to one-dimensional blood flow. *J. Comput. Phys.* **2015**, *300*, 423–437. [CrossRef]
8. Charlton, P.H.; Mariscal Harana, J.; Vennin, S.; Li, Y.; Chowienczyk, P.; Alastruey, J. Modeling arterial pulse waves in healthy aging: A database for in silico evaluation of hemodynamics and pulse wave indexes. *Am. J. Physiol.-Heart Circ. Physiol.* **2019**, *317*, H1062–H1085. [CrossRef] [PubMed]
9. Murillo, J.; García-Navarro, P. A solution of the junction Riemann problem for 1d hyperbolic balance laws in networks including supersonic flow conditions on elastic collapsible tubes. *Symmetry* **2021**, *13*, 1658. [CrossRef]
10. Murillo, J.; García-Navarro, P. Numerical coupling of 0D and 1D models in networks of vessels including transonic flow conditions. Application to short-term transient and stationary hemodynamic simulation of postural changes. *Int. J. Numer. Methods Biomed. Eng.* **2023**, *39*, e3751. [CrossRef] [PubMed]
11. Vallés, P.; Fernández-Pato, J.; Morales-Hernández, M.; Echeverribar, I.; García-Navarro, P. A 2D shallow water flow model with 1D internal boundary condition for subgrid-scale topography. *Adv. Water Resour.* **2024**, *189*, 104716. [CrossRef]
12. Gordillo, G.; Morales-Hernández, M.; García-Navarro, P. Solute transport control at channel junctions using adjoint sensitivity. *Mathematics* **2021**, *10*, 93. [CrossRef]
13. Cunge, J.A.; Holly, F.M.; Verwey, A. *Practical Aspects of Computational River Hydraulics*; Pitman Advanced Publishing Program: Boston, MA, USA, 1980.
14. Gurram, S.K.; Karki, K.S.; Hager, W.H. Subcritical junction flow. *J. Hydraul. Eng.* **1997**, *123*, 447–455. [CrossRef]
15. Hsu, C.C.; Wu, F.S.; Lee, W.J. Flow at 90 equal-width open-channel junction. *J. Hydraul. Eng.* **1998**, *124*, 186–191. [CrossRef]
16. Li, Q.; Liang, Q.; Xia, X. A novel 1D–2D coupled model for hydrodynamic simulation of flows in drainage networks. *Adv. Water Resour.* **2020**, *137*, 103519. [CrossRef]
17. Kesserwani, G.; Ghostine, R.; Vazquez, J.; Mosé, R.; Abdallah, M.; Ghenaim, A. Simulation of subcritical flow at open-channel junction. *Adv. Water Resour.* **2008**, *31*, 287–297. [CrossRef]
18. Rice, C.E. *Open Channel Junctions with Supercritical Flow*; ARS-United States Department of Agriculture, Agricultural Research Service (USA): Washington, DC, USA, 1985.
19. Kesserwani, G.; Ghostine, R.; Vazquez, J.; Ghenaim, A.; Mosé, R. One-dimensional simulation of supercritical flow at a confluence by means of a nonlinear junction model applied with the RKDG2 method. *Int. J. Numer. Methods Fluids* **2008**, *57*, 1695–1708. [CrossRef]
20. Ghostine, R.; Vazquez, J.; Terfous, A.; Mose, R.; Ghenaim, A. Comparative study of 1D and 2D flow simulations at open-channel junctions. *J. Hydraul. Res.* **2012**, *50*, 164–170. [CrossRef]
21. Sherwin, S.J.; Formaggia, L.; Peiro, J.; Franke, V. Computational modelling of 1D blood flow with variable mechanical properties and its application to the simulation of wave propagation in the human arterial system. *Int. J. Numer. Methods Fluids* **2003**, *43*, 673–700. [CrossRef]
22. Goudiaby, M.S.; Kreiss, G. A Riemann problem at a junction of open canals. *J. Hyperbolic Differ. Equ.* **2013**, *10*, 431–460. [CrossRef]
23. Elshobaki, M.; Valiani, A.; Caleffi, V. Junction Riemann problem for one-dimensional shallow water equations with bottom discontinuities and channels width variations. *J. Hyperbolic Differ. Equ.* **2018**, *15*, 191–217. [CrossRef]
24. Alcrudo, F.; Benkhaldoun, F. Exact solutions to the Riemann problem of the shallow water equations with a bottom step. *Comput. Fluids* **2001**, *30*, 643–671. [CrossRef]
25. Toro, E.F. *Riemann Solvers and Numerical Methods for Fluid Dynamics: A Practical Introduction*; Springer Science & Business Media: Berlin/Heidelberg, Germany, 2013.
26. Colombo, R.M.; Herty, M.; Sachers, V. On 2×2 conservation laws at a junction. *SIAM J. Math. Anal.* **2008**, *40*, 605–622. [CrossRef]
27. Murillo, J.; García-Navarro, P. Energy balance numerical schemes for shallow water equations with discontinuous topography. *J. Comput. Phys.* **2013**, *236*, 119–142. [CrossRef]
28. Murillo, J.; Navas-Montilla, A. A comprehensive explanation and exercise of the source terms in hyperbolic systems using Roe type solutions. Application to the 1D–2D shallow water equations. *Adv. Water Resour.* **2016**, *98*, 70–96. [CrossRef]
29. Mairal, J.; Murillo, J.; García-Navarro, P. The Junction Riemann Problem in 1d Shallow Water Channels Including Supercritical Flow Conditions. 2024. Available online: https://papers.ssrn.com/sol3/papers.cfm?abstract_id=5003532 (accessed on 17 February 2025).
30. Murillo, J.; García-Navarro, P. Improved Riemann solvers for complex transport in two-dimensional unsteady shallow flow. *J. Comput. Phys.* **2011**, *230*, 7202–7239. [CrossRef]
31. Echeverribar, I.; Morales-Hernández, M.; Brufau, P.; García-Navarro, P. 2D numerical simulation of unsteady flows for large scale floods prediction in real time. *Adv. Water Resour.* **2019**, *134*, 103444. [CrossRef]
32. Navas-Montilla, A.; Murillo, J. Overcoming numerical shockwave anomalies using energy balanced numerical schemes. Application to the Shallow Water Equations with discontinuous topography. *J. Comput. Phys.* **2017**, *340*, 575–616. [CrossRef]